Ozone trends derived from the total column and vertical profiles at a northern mid-latitude station

Prijitha J. Nair, Sophie Godin-Beekmann, Jayanarayanan Kuttippurath, Gérard Ancellet, Florence Goutail, Andrea Pazmino, L. Froidevaux, J. M. Zawodny, R. D. Evans, H. J. Wang, et al.

Atmos. Chem. Phys., 13, 10373–10384, 2013
www.atmos-chem-phys.net/13/10373/2013/
doi:10.5194/acp-13-10373-2013

Atmospheric Chemistry and Physics Open Access

Ozone trends derived from the total column and vertical profiles at a northern mid-latitude station

P. J. Nair[1], S. Godin-Beekmann[1], J. Kuttippurath[1], G. Ancellet[1], F. Goutail[1], A. Pazmiño[1], L. Froidevaux[2], J. M. Zawodny[3], R. D. Evans[4], H. J. Wang[5], J. Anderson[6], and M. Pastel[1]

[1]UPMC Université Paris 06, Université Versailles-Saint-Quentin, UMR 8190, LATMOS-IPSL, CNRS/INSU, Paris, France
[2]Jet Propulsion Laboratory, California Institute of Technology, Pasadena, CA, USA
[3]Chemistry and Dynamics Branch, NASA Langley Research Center, Hampton, VA, USA
[4]NOAA, Earth System Research Laboratory, Global Monitoring Division, Boulder, Colorado, USA
[5]Georgia Institute of Technology, Atlanta, GA, USA
[6]Hampton University, Hampton, VA, USA

Correspondence to: P. J. Nair (gopalapi@aero.jussieu.fr)

Received: 17 February 2013 – Published in Atmos. Chem. Phys. Discuss.: 18 March 2013
Revised: 19 August 2013 – Accepted: 5 September 2013 – Published: 24 October 2013

Abstract. The trends and variability of ozone are assessed over a northern mid-latitude station, Haute-Provence Observatory (OHP: 43.93° N, 5.71° E), using total column ozone observations from the Dobson and Système d'Analyse par Observation Zénithale spectrometers, and stratospheric ozone profile measurements from light detection and ranging (lidar), ozonesondes, Stratospheric Aerosol and Gas Experiment (SAGE) II, Halogen Occultation Experiment (HALOE) and Aura Microwave Limb Sounder (MLS). A multivariate regression model with quasi-biennial oscillation (QBO), solar flux, aerosol optical thickness, heat flux, North Atlantic Oscillation (NAO) and a piecewise linear trend (PWLT) or equivalent effective stratospheric chlorine (EESC) functions is applied to the ozone anomalies. The maximum variability of ozone in winter/spring is explained by QBO and heat flux in the ranges 15–45 km and 15–24 km, respectively. The NAO shows maximum influence in the lower stratosphere during winter, while the solar flux influence is largest in the lower and middle stratosphere in summer. The total column ozone trends estimated from the PWLT and EESC functions are of -1.47 ± 0.27 and -1.40 ± 0.25 DU yr^{-1}, respectively, over the period 1984–1996 and about 0.55 ± 0.30 and 0.42 ± 0.08 DU yr^{-1}, respectively, over the period 1997–2010. The ozone profiles yield similar and significant EESC-based and PWLT trends for 1984–1996, and are about -0.5 and -0.8 % yr^{-1} in the lower and upper stratosphere, respectively. For 1997–2010, the EESC-based and PWLT estimates are of the order of 0.3 and 0.1 % yr^{-1}, respectively, in the 18–28 km range, and at 40–45 km, EESC provides significant ozone trends larger than the insignificant PWLT results. Furthermore, very similar vertical trends for the respective time periods are also deduced from another long-term satellite-based data set (GOZCARDS–Global OZone Chemistry And Related trace gas Data records for the Stratosphere) sampled at northern mid-latitudes. Therefore, this analysis unveils ozone recovery signals from total column ozone and profile measurements at OHP, and hence in the northern mid-latitudes.

1 Introduction

After two decades of regulated emissions, the level of stratospheric ozone depleting substances (ODSs) has been reduced, and some of its components have been phased out (WMO, 2007). The analyses show that total column ozone measurements in the mid-latitudes are stabilised from the mid-1990s onwards (Newchurch et al., 2003; Reinsel et al., 2005; Vyushin et al., 2007). Similarly, a significant change in trend is found in the upper stratosphere at mid-latitudes (Steinbrecht et al., 2006; Jones et al., 2009). Thus, stratospheric ozone showed a slowing of decline attributable to ODS decrease at mid-latitudes (WMO, 2011).

Since 1990, several studies have focused on the interannual variability of ozone in connection with the seasonal cycle, quasi-biennial oscillation (QBO), solar flux and aerosol optical thickness (Bojkov et al., 1990; Reinsel et al., 1994; Staehelin et al., 1998). In the recent decade the dynamical variations using heat flux, a proxy describing the planetary wave drive, are discussed to investigate changes in ozone distributions related to the residual circulation (Dhomse et al., 2006; Weber et al., 2011). The teleconnection patterns such as North Atlantic Oscillation (NAO) and Arctic Oscillation (AO) also have significant influence on ozone, particularly in the middle stratosphere (Weiss et al., 2001). The long-term trend in ozone has been estimated using various methods including piecewise linear trend (PWLT) (Reinsel et al., 2002, 2005; Zanis et al., 2006; Vyushin et al., 2007, 2010; Kuttippurath et al., 2013) and equivalent effective stratospheric chlorine (EESC) functions and EESC-dependent functions (Yang et al., 2006; Brunner et al., 2006; Wohltmann et al., 2007; Kiesewetter et al., 2010; Salby et al., 2011).

This study analyses the trends and variability in total column ozone and stratospheric ozone profiles at Haute-Provence Observatory (OHP: 43.93° N, 5.71° E). A regression model with various explanatory parameters such as QBO, solar flux, aerosol optical thickness, heat flux, NAO and EESC or PWLT functions is applied to the data. Total column ozone observations from the Dobson and Système d'Analyse par Observation Zénithale (SAOZ) spectrometers and ozone profile measurements from the light detection and ranging (lidar), ozonesondes, Stratospheric Aerosol and Gas Experiment (SAGE) II, Halogen Occultation Experiment (HALOE) and Aura Microwave Limb Sounder (MLS) are used for the study. We have tested the regression method and trend estimates with another long-term merged ozone data set, GOZCARDS (Global OZone Chemistry And Related trace gas Data records for the Stratosphere). This data set was accessed from the Goddard Earth Sciences Data and Information Services Center (GES DISC) at http://disc.sci.gsfc.nasa.gov. The reference and digital object identifier (DOI) for this particular GOZCARDS product are provided by Wang et al. (2013).

This article is organised as follows: the descriptions of total column ozone, ozone vertical profiles, explanatory variables and the regression model are given in Sect. 2. Section 3 discusses the regression analyses, variability and trends derived from both total column and vertically resolved ozone profiles. Finally, Sect. 4 concludes with the main findings.

2 Data and methods

2.1 Total column ozone observations

The measurement principle of Dobson spectrometer is based on the differential absorption of solar light by ozone (Dobson, 1957, 1968). It performs ozone observations by measuring the relative intensities of ultraviolet (UV) wavelengths emanating from the Sun, Moon or zenith sky. At OHP, Dobson column data are derived from the direct sun and zenith sky observations, in which 83 % are from the direct sun observations. The precision and accuracy of direct sun observations are ∼ 1 % and ∼ 3 %, respectively, while the zenith observations are less precise (Basher et al. (1982) and http://www.esrl.noaa.gov/gmd/ozwv/dobson/papers/report13/report13.html). We use Dobson total column ozone measurements for the 1984–2010 period (http://woudc.org/data/citation_e.html).

SAOZ observes sunlight scattered from the zenith sky in the 300–600 nm spectral range during sunrise and sunset (Pommereau and Goutail, 1988). Ozone measurements are carried out in the Chappuis band (450–650 nm) and are retrieved using differential optical absorption spectroscopy method. The SAOZ version (v) 2 data for 1992–2010 are used here. The measurement uncertainty is of the order of 3 % (Hendrick et al., 2011).

2.2 Ozone profile measurements

The lidar instrument at OHP uses the differential absorption lidar technique for measuring ozone with the ozone-absorbed wavelength at 308 nm and the non-absorbed wavelength at 355 nm. The uncertainty of the measurements is ∼ 5 % below 20 km, 3 % at 20–45 km and 10 % above 45 km. The important features of the OHP ozone lidar measurements are described in Godin-Beekmann et al. (2003) and Nair et al. (2011, 2012). Lidar ozone measurements during the period 1985–2010 are used for the study.

At OHP, electrochemical concentration cell (ECC) ozonesondes (Komhyr, 1969) with 1 % buffered potassium iodide cathode sensor solution have been used since 1991. We follow the approach described in Nair et al. (2012) for analysing the ozonesonde data. The vertical resolution of the sonde measurements is ∼ 0.2 km and the uncertainty is ±5–10 % up to ∼ 32 km (Smit et al., 2007). The ECC ozonesonde profiles over the 1991–2010 period are utilised for the analysis.

SAGE II, on the Earth Radiation Budget Satellite, uses the solar occultation technique for measuring ozone. These ozone measurements have a vertical resolution of ∼ 1 km with an uncertainty of ∼ 5 % at 20–45 km and 5–10 % at 15–20 km (Wang et al., 2006). The ozone number density profiles processed by the v7.0 algorithm for the period 1984–2005 are considered here.

HALOE, on the Upper Atmosphere Research Satellite (UARS), used the solar occultation technique for measuring ozone from the limb transmittances of the 9.6 µm ozone band (Russell et al., 1993). The vertical resolution of ozone profiles is ∼ 2.5 km with an uncertainty of 10 % at 30–64 km and ∼ 30 % at 15 km (Brühl et al., 1996). The ozone volume

mixing ratio (VMR) profiles v19 for 1991–2005 are used for the analysis.

Aura MLS measures thermal emissions from the rotational lines of the measured species through the limb of the atmosphere. Ozone measurements have a vertical resolution of 2.5–3 km in the stratosphere and an uncertainty of 5–10 % between 16 and 60 km (Froidevaux et al., 2008). The ozone VMRs from Aura MLS v3.3 for 2004–2010, screened as suggested in the v3.3 validation report (Livesey et al., 2011), are used here. Table 1 summarises the important characteristics of different instruments used for the study. These include the periods considered for the analysis and the measurement frequency of various data sets, vertical resolution and vertical range of the profile measurements, and the latitude and longitude bands chosen for the satellite data sets to find closest profiles at the station location.

2.3 Explanatory variables

Several proxies are used to diagnose, for instance, the changes in ozone associated with the natural and anthropogenic variations. The QBO (http://www.geo.fu-berlin.de/en/met/ag/strat/produkte/) is a quasi-periodic oscillation of the equatorial zonal wind (Andrews et al., 1987). Since the QBO is of equatorial origin, its effect on ozone is in different phases at various latitudes (Bojkov et al., 1990). In our study, we use Singapore zonal winds at 10 and 30 hPa (hereafter QBO 10 and QBO 30, respectively), which are out of phase by $\sim \frac{\pi}{2}$ (Steinbrecht et al., 2003). Monthly mean solar flux observations (ftp://ftp.ngdc.noaa.gov/STP/SOLAR_DATA/SOLAR_RADIO/FLUX/) at a wavelength of 10.7 cm made at Ottawa and Penticton are used for investigating the impact of 11 yr solar-cycle-related variations of UV irradiance on ozone. The effect of volcanic aerosols (http://data.giss.nasa.gov/modelforce/strataer/) on ozone is studied using the aerosol optical thickness measured at 550 nm (Sato et al., 1993).

To account for the effect of Brewer–Dobson circulation, planetary wave activity from the troposphere to stratosphere is analysed using the heat flux data averaged over the range 45–75° N at 100 hPa, as described in Kuttippurath and Nikulin (2012). The cumulative heat flux is calculated for a given month by integrating the heat flux from the preceding October to the month concerned, keeping the data for October as such (e.g. Dhomse et al., 2006). The NAO (http://www.cru.uea.ac.uk/cru/data/) is another proxy affecting the Northern Hemisphere climate (Hurrell et al., 2003). It is measured as the difference between the normalised sea level pressure over Gibraltar and southwest Iceland (e.g. Appenzeller et al., 2000). To account for the influence of ODS abundances, EESC (http://fmiarc.fmi.fi/candidoz/) is used as a proxy. The EESC trends are estimated to be about 0.05 and $-0.02\,\mathrm{ppbyr}^{-1}$ before and after the EESC peak year (1997 in the mid-latitudes), respectively (Vyushin et al., 2010).

2.4 Multiple regression model

The long-term evolution of monthly mean ozone is analysed using a regression model, which is similar to those of Reinsel et al. (1994), Staehelin et al. (1998) and Kuttippurath et al (2013). Our analysis adopts two different methodologies to assess the trend. First, the PWLT function is used for estimating ozone trends before and after 1997, and is referred to as the PWLT model (Reinsel et al., 2002). Secondly, the EESC function is used instead of the PWLT terms in the model and is called the EESC-based model (Brunner et al., 2006). In this study, PWLTs are estimated using the turn-around year of 1997 as EESC peaks in 1997 at mid-latitudes (WMO, 2011). The selection of the turn-around year is very important as it affects largely the PWLT results.

The regression model is fitted to ozone time series of each month (January, February, ..., December) over the period. Variations in ozone (Y) due to the natural and anthropogenic changes can be expressed as

$$Y(t) = \sum_{m=1}^{12} C_m^X X(t) + \epsilon(t),$$

where C_m^X is the regression coefficient of the proxy (X) time series for each month m (January, February, ..., December), t corresponds to the months in the time series and ϵ is the residual.

In the regression, monthly mean QBO, solar flux, aerosols and NAO and deseasonalised heat flux are used. The error of regression coefficient is calculated as (Press et al., 1989)

$$\sigma_c^2 = (\mathbf{A}^T\mathbf{A})^{-1} \times \frac{\sum_t \left(Y(t) - \sum_{m=1}^{12} C_m^X X(t) \right)^2}{Z - P} \times \frac{1+\phi}{1-\phi}$$

where $\mathbf{A}$ is the matrix of the proxies, Z is the number of data points, P is the number of fitted parameters and ϕ is the autocorrelation of the residuals.

3 Results and discussion

3.1 Regression analysis of column ozone

The temporal evolution of the total column ozone measurements from the Dobson and SAOZ spectrometers is displayed in Fig. 1a. Both data sets follow a similar pattern of ozone evolution. Ozone values are relatively lower after the early 1990s and level off after the early 2000s. A maximum ozone value of about 420 DU is observed in 2010 as found by the Dobson spectrometer. The deseasonalised (monthly mean ozone – monthly climatology over the period) total column ozone measurements are used for the regression analysis. There are slight differences between the two data sets in June and July. These seasonal differences are removed by

Table 1. The different instruments used for the analysis along with the analysis period, frequency of ozone measurements, vertical resolution (Ver. Res.), measurement range and the latitude and longitude bands (Lat., Long.) chosen for the satellite instruments to find the profiles near OHP (43.93° N, 5.71° E).

Measurement Type	Instruments	Analysis Period	Measurement Frequency	Ver. Res. (km)	Measurement Range (km)	Lat., Long. (°N; °E)
Column	Dobson	1984–2010	20 month^{-1}	-	-	-
	SAOZ	1992–2010	30 month^{-1}	-	-	-
Profile	Ozonesondes	1991–2010	5 month^{-1}	0.2	0–32	-
	LIDAR	1985–2010	15 month^{-1}	0.5–2 (<31 km)	26–43 (<1994)	-
				2–4.5 (31–45 km)	12–45 (>1993)	
	SAGE II	1984–2005	30 day^{-1}	1.0	5–70	±5; ±10
	HALOE	1991–2005	30 day^{-1}	2.5	10–90	±5; ±10
	Aura MLS	2004–2010	3500 day^{-1}	2.5–3	10–75	±2.5; ±5

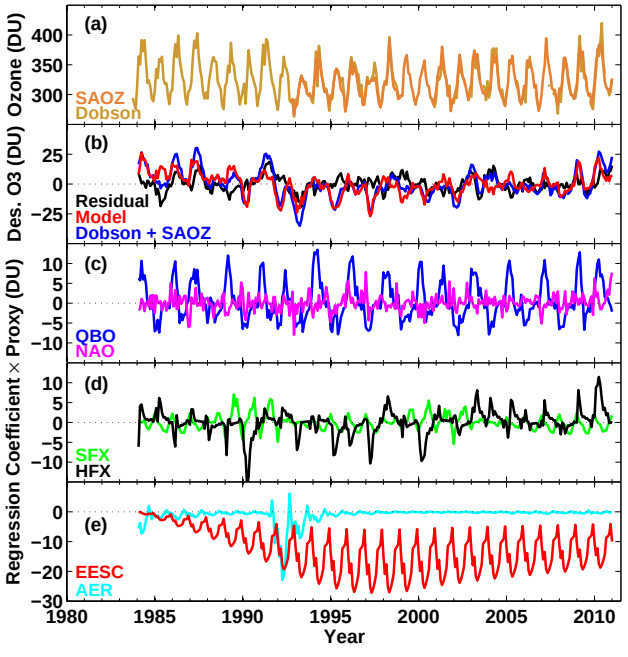

Fig. 1. (a) Time series of the total column ozone measurements from the Dobson and SAOZ spectrometers; **(b)** monthly mean deseasonalised ozone, the EESC-based model and the residual; **(c)** ozone-fitted signals of proxies QBO and NAO; **(d)** solar flux (SFX) and heat flux (HFX); and **(e)** aerosols (AER) along with the EESC fit.

deseasonalising the data. The deseasonalised data from both instruments are averaged during the overlapping period, as listed in Table 1, to obtain a single data set from 1984 to 2010. The comparison between Dobson and SAOZ column measurements shows a drift of about $-0.12\,\%\,\mathrm{yr}^{-1}$, while the combined long-term data show much smaller drift of about $0.05\,\%\,\mathrm{yr}^{-1}$. This analysis suggests that the combined data from Dobson and SAOZ observations provide relatively stable long-term data compared to the individual Dobson or SAOZ measurements, and a stable data set is a prerequisite

Table 2. The regression coefficients of QBO 10, QBO 30, solar flux (SFX), NAO, heat flux (HFX) and volcanic aerosols estimated from the total column ozone measurements, shown for April, November and the average of all months. The QBO 10 and QBO 30 are expressed in DU $(\mathrm{ms}^{-1})^{-1}$, solar flux in DU (100 solar flux unit)$^{-1}$, heat flux in DU $(\mathrm{K\,ms}^{-1})^{-1}$, aerosol and NAO are given in DU. Twice the standard deviation of the regression coefficient is also given.

Proxy	Apr	Nov	Average
QBO 10	-0.09 ± 0.25	-0.07 ± 0.14	-0.07 ± 0.05
QBO 30	-0.17 ± 0.29	$+0.03 \pm 0.18$	-0.06 ± 0.06
SFX	$+1.44 \pm 9.50$	-2.15 ± 5.59	$+1.42 \pm 1.97$
NAO	$+1.49 \pm 3.17$	-1.76 ± 1.73	-0.47 ± 0.65
HFX	$+5.52 \pm 5.62$	$+0.59 \pm 1.96$	$+2.49 \pm 1.32$
Aerosol	-148.68 ± 159.51	-39.47 ± 116.91	-67.52 ± 36.17

for accurate trend estimations. This data set is smoothed using a 5-month running mean, and then the multiple regression analysis is performed. The deseasonalised ozone, the fitted regression model and residuals are shown in Fig. 1b. The regression model explains about 65 % of the variance in the total column ozone, as estimated from the R^2 statistics (Storch and Zwiers, 1999), and the autocorrelation is ~ 0.12 for 1 yr lag. Table 2 provides the regression coefficients of all explanatory variables estimated for the months of April and November, when the ozone trend estimates show maximum and minimum values, respectively, and the average of all months.

The explanatory parameters fitted to the data are displayed in Fig. 1c–e. Generally QBO, solar flux, heat flux and NAO together explain most of the ozone variations. For instance, the easterly phase of QBO and negative NAO index contribute to the large ozone values in 1986 and 1987. The ozone decrease in 1990 and 2002 is well captured by the model, and is largely influenced by the westerly phase of QBO, positive NAO index and small heat flux, even if solar maximum should increase the ozone amount. The aerosol terms

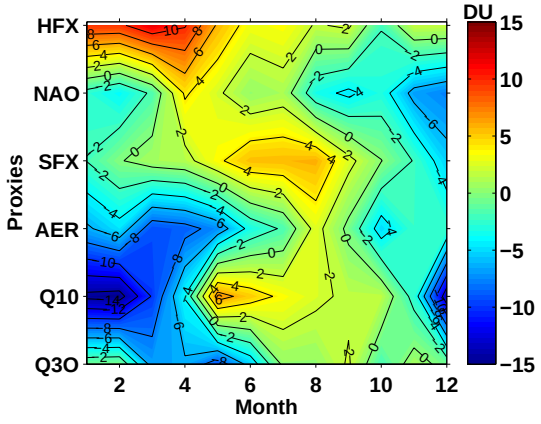

Fig. 2. The influence of individual explanatory variables on the variability of combined Dobson and SAOZ total column ozone data analysed using the EESC-based model. The Q30 and Q10 represent QBO 30 and QBO 10, respectively.

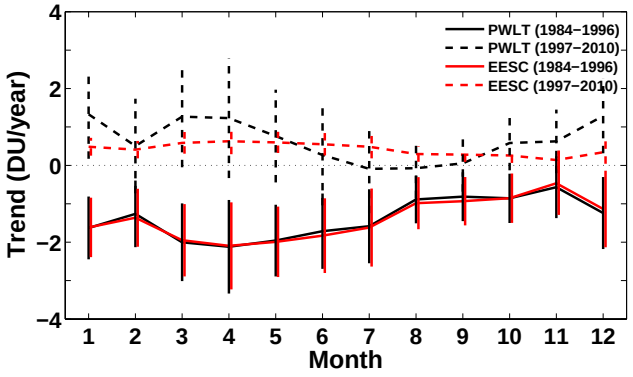

Fig. 3. The monthly ozone trends derived from the combined Dobson and SAOZ total column ozone measurements. The black and red curves represent the PWLTs and EESC-based ozone trends, respectively. The solid and dashed lines denote ozone trends over the periods 1984–1996 and 1997–2010, respectively. The error bars correspond to the 95 % confidence intervals.

associated with the Mount Pinatubo eruption contributed to about 25 DU decrease in total ozone in 1993.

The large ozone values in 2010 are well explained by the model with large QBO (12 DU), heat flux (9 DU) and NAO (6 DU). A recent study by Steinbrecht et al. (2011) reported that the easterly phase of QBO and a large negative AO index resulted in the large value of ozone observed at the Meteorological Observatory Hohenpeissenberg, another northern mid-latitude station near OHP. Our study confirms their findings, but it also points out that the large planetary wave activity during the period also contributed to this anomalous ozone value. Similarly, large ozone values in 2009 can be explained by the coincidence of easterly phase of QBO ($\sim$ 12 DU) and large heat flux ($\sim$ 9 DU).

The influence of proxies on the inter-annual variability of ozone is presented in Fig. 2. It is estimated as $C_m^X \times 2\sigma(X)$ with σ as the standard deviation of the proxy time series (Steinbrecht et al., 2003). The positive values show correlation between the proxy and ozone data, while negative values exhibit anticorrelation. A proxy term is considered to be significant if the regression coefficient of a proxy is greater than twice the standard deviation of the respective proxy.

In Fig. 2, Q10 and Q30 are the individual contributions of QBO 10 and QBO 30, respectively. In general, QBO 10 and QBO 30 exhibit an anticorrelation with ozone in the period November–May and provide significant contribution of about 12 and 8 DU, respectively, to the ozone variability. The aerosol proxy data show an anticorrelation with ozone in all months and explain about 10 DU of the ozone variability. The solar flux correlates with ozone and shows a significant variability of about 5 DU in summer. Similarly, NAO shows a correlation in spring and anticorrelation in other seasons, with a maximum variability of about 6 DU in November. The heat flux shows positive correlation, and is significant in winter, contributing about 8 DU to the ozone variability.

3.1.1 Trends in total column ozone

Figure 3 presents the seasonal evolution of ozone trends estimated from the PWLT and EESC-based models before and after 1997. The ozone trends estimated before 1997 based on the PWLT and EESC fits are negative and similar. The EESC-based ozone trends calculated after 1997 are significantly positive in all months. Similarly, the PWLT estimates are significant in all months except for July and August. It is reported that the increase of ozone after the EESC-peak year is largely influenced by the dynamics (WMO, 2011). Therefore, the negative PWLTs estimated for July–August can be attributed to the lower planetary wave drive during the summer compared to that in winter and spring seasons. In addition, a clear seasonality is observed in both trends, with the maximum in winter/spring. For 1984–1996, maximum PWLT and EESC-based ozone trend is found in April and minimum in November. For 1997–2010, the maximum PWLT is computed in March and minimum in August, while the EESC-based ozone trend is maximum in April and minimum in November. Please note that 2-σ error bars are provided elsewhere in the text.

Table 3 lists the year-round total column ozone trends estimated from the PWLT and EESC-based regression models. The PWLT fits provide significant year-round trend of -1.47 ± 0.27 DU yr^{-1} over the period of 1984–1996 and 0.55 ± 0.30 DU yr^{-1} over that of 1997–2010. The ozone trends using EESC fits are -1.40 ± 0.25 DU yr^{-1} over the 1984–1996 period and 0.42 ± 0.08 DU yr^{-1} between 1997 and 2010. It should be noted that the PWLT prior to 1997 coincides with the trend estimated using EESC function, while the PWLT after 1997 is larger than the trend computed using the EESC fit. It suggests that in the considered latitude regimes, the decrease in total ozone before 1997 is attributed to the increased ODS abundances, while the increase in total

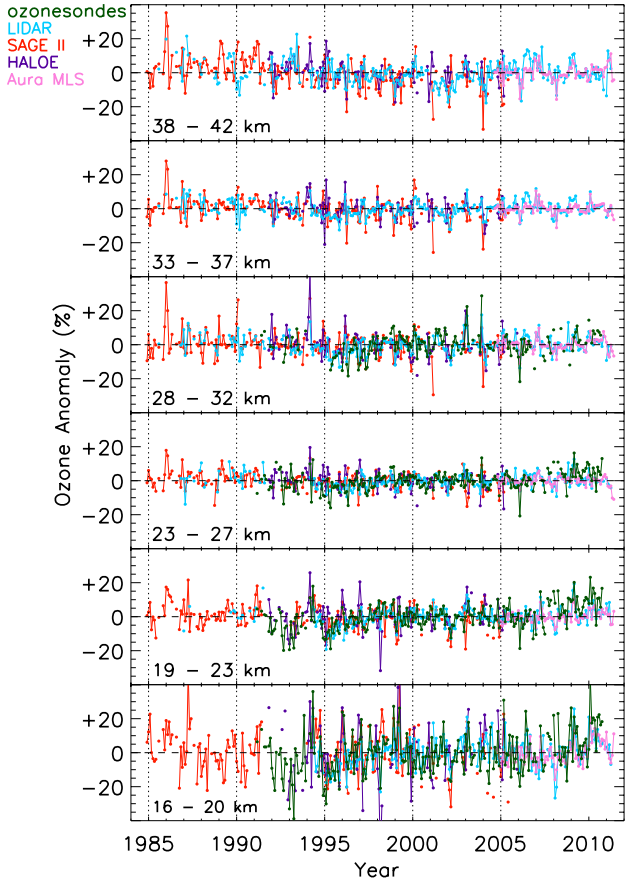

Fig. 4. Time series of ozone anomalies at OHP estimated from lidar, ozonesondes, SAGE II, HALOE and Aura MLS ozone measurements at specific altitude bands. The data are resolved on a 1 km vertical grid.

ozone after the turn-around year can partly be explained by the decreased amount of ODSs, consistent with the previous studies (WMO, 2011). This suggests the influence of known or unknown parameters (including dynamics) along with the ODS decrease for the significant positive trends in the 1997–2010 period. Note that a detailed discussion of most known proxies that have significant influence on the mid-latitude ozone is presented in Mäder et al. (2007). A similar result is shown by Vyushin et al. (2007) from the Total Ozone Mapping Spectrometer and Solar Backscatter UltraViolet zonal average data analysed using both PWLT and EESC fits in the northern mid-latitudes.

We have also tested the regression method using some additional proxies. For instance, an analysis performed with QBO 30 and QBO 50 (QBO at 50 hPa) yields trend values within 2 % of the standard scenario presented above. Since QBO 50 is mainly used for studying near-tropopause variations, we applied QBO 10 instead of QBO 50 in the regression procedure. In addition, we have also tried the El Niño–Southern Oscillation (ENSO) and NAO together in the regression analysis. The resulting trend values stayed within 3 % and well within the uncertainties of the standard procedure given in Table 3. As ENSO and NAO have a cross-coherency (and correlation) due to the influence of ENSO on NAO (e.g. Huang et al., 1998), we did not use both proxies together in the standard regression analyses presented in this study.

Table 3. The year-round total column ozone trends in DU yr^{-1} with 95 % confidence intervals estimated from both PWLT and EESC fits.

Method	1984–1996	1997–2010
PWLT	-1.47 ± 0.27	0.55 ± 0.30
EESC	-1.40 ± 0.25	0.42 ± 0.08

3.2 Regression analysis of ozone profiles

The ozone profile measuring instruments such as lidar, ozonesondes, SAGE II, HALOE and Aura MLS are used for finding the evolution of stratospheric ozone between 1984 and 2010. The SAGE II and HALOE ozone measurements are taken within ±5° latitude and ±10° longitude bands with respect to the location of OHP, while Aura MLS ozone observations within ±2.5° latitude and ±5° longitude box around the station are used. The other screening criteria mentioned in Nair et al. (2011, 2012) are also applied here for various measurements. Since these data sets have different vertical resolution, they are interpolated into a 1 km vertical grid.

Figure 4 shows the monthly ozone anomaly in percent [100× (monthly mean ozone − monthly climatology)/monthly climatology] of each measurement technique at the altitude bands of 16–20, 19–23, 23–27, 28–32, 33–37 and 38–42 km. All measurement techniques exhibit similar ozone anomalies and are within ±10 % generally, except at 16–20 km. Similarly, ozone anomalies are slightly higher at 38–42 km before the mid-1990s. In 2010, all available data sets show positive anomalies at 16–20 km, which implies that a major part of the total column ozone in 2010, noted in Sect. 3.1, arises from the lower stratosphere.

The estimated ozone anomalies in 1 km grid are used for the multiple regression analysis from 15 to 45 km. The ozone anomalies in the running month during the overlapping periods of various instruments are averaged to form a single profile in a month. These combined data show insignificant drifts of less than ± 0.3 % yr^{-1} at 15–45 km. It should be noted that a detailed analysis of the drifts of individual data sets is given in our previous publications (Nair et al., 2011, 2012). These merged data are smoothed using a 5-month running mean and then regressed. The same regression models and proxies used for the analysis of total column ozone measurements are used here. However, the aerosol proxy data are applied only up to 30 km as they are not important above 30 km due to the decrease in surface area density.

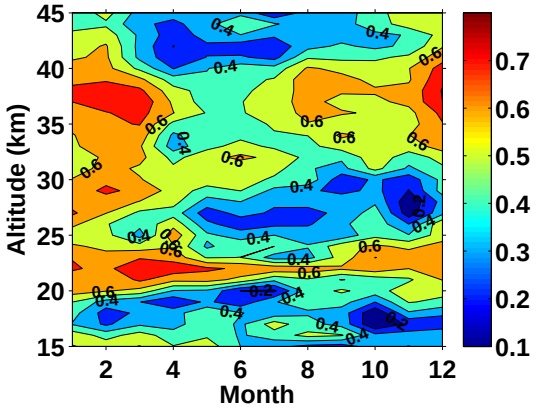

Fig. 5. Seasonal variations of the vertical distribution of R^2 estimates computed for the average of the stratospheric ozone anomalies at OHP from different observations.

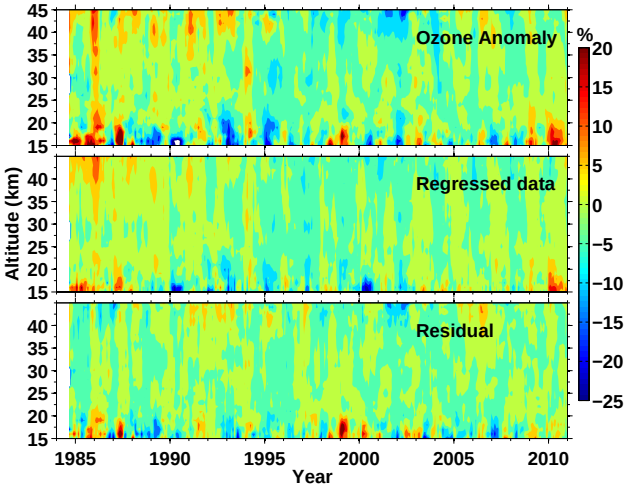

Fig. 6. Temporal evolution of the vertical distribution of average ozone anomaly (top panel), regression model (middle panel) and residual (bottom panel) at OHP over the period 1984–2010.

In order to find how well the model explains the observed variability of the ozone, R^2 is calculated in each month for the EESC-based model, and is shown in Fig. 5. The 5-month smoothing generally increases the correlation between ozone anomaly and the model because smoothing reduces the discontinuity of ozone anomaly time series and suppresses unreasonable peaks. The model shows a good agreement in the 20–40 km region in all months except around 25 km in the summer and autumn months. The best agreement is found in the winter/spring months, with R^2 values greater than 0.6 above 20 km, and reaching about 0.85 at 22 km in March and April. On the other hand, the model explains only 20–50 % of the variability over the range 16–18 km over all months, indicating that the considered proxies are not sufficient to explain the observed variability at these altitudes.

Figure 6 displays the vertical distribution of the temporal evolution of average ozone anomaly (top panel), the EESC-based model (middle panel) and the residual (bottom panel). The observed features in the ozone anomaly are reproduced quite well in the regressed data between 20 and 40 km, and the corresponding residuals are nearly zero. Large positive ozone anomalies are found in the whole stratosphere in 1986 and negative ones for 1995–1997. These features are more or less replicated by the model with wave activity, QBO and NAO. Low-ozone anomalies are estimated in the lower stratosphere in 1989, 1993, 1995 and 2002, and can be explained in part due to large positive NAO indices in those years. Additionally, an about 15 % reduction in ozone in 1993 is associated with aerosols from the Mount Pinatubo volcanic eruption.

Large positive ozone anomalies are observed in the lower stratosphere in 1987, 1999, 2009 and 2010. The regression model could explain a part of these large ozone anomalies in 1987 and 2009, which is caused by the easterly phase of QBO and large negative NAO index. The model reproduces well the large ozone anomaly in the lower stratosphere in 2010, which is contributed by the large planetary wave activity, the easterly phase of QBO, and the negative NAO index, as discussed for the total column ozone. In contrast, the considered proxies could not explain very high ozone found in the lower stratosphere in 1999. This is due to the fact that the Arctic winter of 1999 was characterised by an unusually warm polar vortex, and the vortex filaments were elongated down to southern Europe (e.g. Heese et al., 2001; Godin et al., 2002).

3.2.1 Link between ozone profile and total column

To find the altitude range from which the explanatory variables contribute the most to total column ozone, a regression analysis is performed to the ozone vertical profiles in DU km^{-1}. The estimated variabilities of the proxies are integrated in 1 km widths, and are shown in Fig. 7. Therefore, this figure can be compared to the variability of proxies contributing to the total ozone variability (i.e. Fig. 2).

The contribution of various proxies is distinct at different altitude ranges. For instance, both QBO 30 and QBO 10 show negative and positive correlations with total ozone from November to April and from May to October, respectively (see Fig. 2). In comparison to Fig. 7, it is found that maximum contribution ($\sim$ 3–8 DU) of QBO 30 to the total ozone comes from the lower stratosphere (15–24 km), whereas the maximum contribution (3–13 DU) of QBO 10 comes from 15 to 35 km. The analysis on ozone profiles and total column ozone observations shows a maximum contribution of QBO 30 in May.

Aerosols show a significant negative correlation with ozone below 22 km and positive correlation above around 22 km. The increase in ozone over the 23–30 km range can be due to the lower concentration of NO_x resulting from the heterogeneous reactions occurring on the surfaces of aerosols

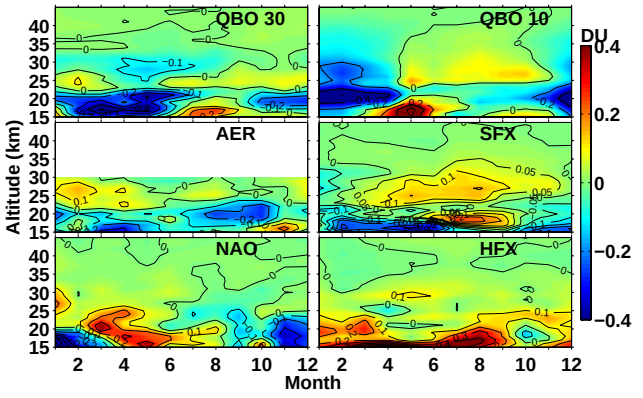

Fig. 7. Variability of different proxies in DU estimated from average ozone anomalies of the vertical profiles at OHP.

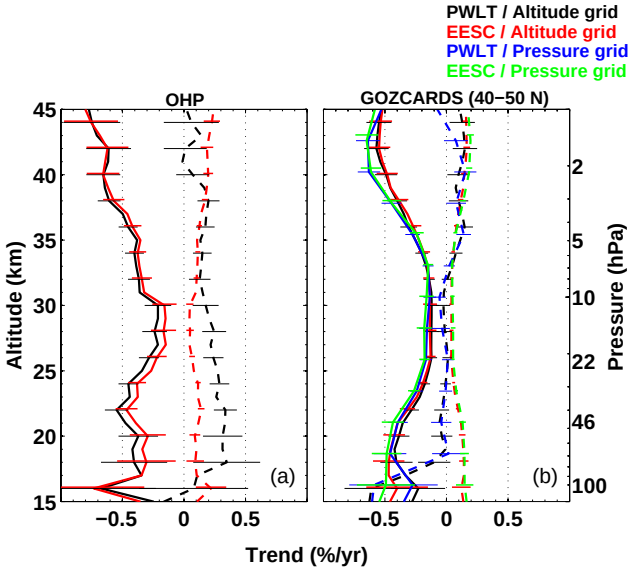

Fig. 8. (a) Vertical structure of the year-round PWLT (black) and EESC-based (red) ozone trends over the range 15–45 km estimated from average ozone anomalies from the OHP-related data sets. **(b)** The PWLT (black) and EESC-based (red) ozone trends estimated on an altitude grid in 1 km spacing and PWLT (blue) and EESC-based (green) trends calculated on GOZCARDS pressure grid from the GOZCARDS monthly ozone anomalies for 40–50° N. The solid and dashed lines represent ozone trends over the periods 1984–1996 and 1997–2010, respectively. The dotted lines represent −0.5, 0 and 0.5 % yr^{-1}. The error bars denote twice the standard deviation.

(e.g. Brunner et al., 2006). The aerosols show maximum correlation with total column and ozone profiles in March. The main contribution of solar flux to total ozone (2–3 DU) arises from the 20–34 km range. A maximum contribution of about 4 DU comes from the 15–34 km range in June–September and from 15–24 km over the period October–May. The maximum variability of total column ozone and profile measurements due to solar flux is found in August.

The NAO provides a contribution of about 5 DU to the total ozone from 15 to 24 km in January–May and in December. In the winter months, NAO index is anticorrelated with ozone as reported in Zanis et al. (2006). The NAO shows its maximum correlation with ozone profiles and total column ozone in the months of December and January. The significant contribution of heat flux to the ozone variability of about 5–8 DU originates from the 15–24 km altitude range. The maximum ozone variability due to heat flux is found in March–April for both total column and profile measurements.

3.2.2 Trends in stratospheric ozone profiles

Figure 8 (a) represents the vertical distribution of year-round ozone trends estimated from the PWLT and EESC fits for 1984–1996 (solid line) and 1997–2010 (dashed line) for average ozone anomaly time series at OHP. For 1984–1996, both trends show similar and significant values of the order of −0.65 % yr^{-1} at 16 km, −0.4 to −0.5 % yr^{-1} at 34–37 km and about −0.8 % yr^{-1} at 38–45 km. In the 17–24 km region, EESC-based and PWLT trends vary slightly and are about −0.5 and −0.4 % yr^{-1}, respectively. The largest negative trends are computed in the 38–45 km region, similar to those estimated in Steinbrecht et al. (2009) and Jones et al. (2009). In the 1997–2010 period, significant ozone trend of 0.3 % yr^{-1} is computed using the PWLT model in the 18–28 km range and of 0.1 % yr^{-1} by the EESC-based model in that of 15–30 km. In the 31–39 km region both regressions yield a similar and significant trend of 0.15 % yr^{-1}. Above 39 km, EESC-based trends are significant and are about 0.25 % yr^{-1}, while PWLT estimates are smaller and insignificant. These results match well with those reported in WMO (2011) and by Vigouroux et al. (2008), who deduced a partial column ozone trend of 0.3 % yr^{-1} at 18–27 and 27–42 km using Fourier transform infrared measurements at Jungfraujoch, another northern mid-latitude station near OHP, for the 1995–2004 period. To check the consistency between the ozone trends estimated from the total column and profile measurements, the ozone trends in DU km^{-1} yr^{-1} are averaged between 10 and 50 km. The resulting EESC-based and PWLT estimates are about −1.0 and −1.1 DUyr^{-1}, respectively, over the period 1984–1996. For 1997–2010 they are of the order of 0.3 and 0.55 DUyr^{-1}, respectively. These results are nearly same as those found for the total column ozone observations.

We have seen a clear signature of ozone recovery from the analysis of profile measurements. Therefore, in order to check the robustness of the method and estimated vertical trends, we have also used an additional data set, GOZCARDS, constructed from various satellite observations. Further details about this recently released (and publicly available) GOZCARDS data set (for ozone and other species) can be found in Froidevaux et al. (2013). In brief,

these merged monthly mean time series adjust zonal mean ozone data sets to the SAGE II data set (as a reference), using data from HALOE and Aura MLS, as well as from the UARS MLS and the Atmospheric Chemistry Experiment Fourier transform spectrometer (ACE-FTS) in addition to SAGE II data. The data set is available as VMRs on a pressure grid. For the analysis, this is converted to number density using GOZCARDS temperature data. The GOZCARDS temperature data set was constructed from monthly zonal means based on Modern-Era Retrospective analysis for Research and Applications (MERRA). Rienecker et al. (2011) provide more information about MERRA (see also http://gmao.gsfc.nasa.gov/merra). Pressure–altitude conversion is made using data from HALOE and Aura MLS and a mean altitude is computed for 1991–2010. The regression is done using monthly ozone anomalies on a vertical grid with 1 km spacing.

Ozone trends derived from this zonal mean data set averaged over the latitude bands 40–50° N using both PWLT (black) and EESC (red) regressions over the periods 1984–1996 and 1997–2010 are shown in Fig. 8 (b). The analysis exhibits similar and significant negative trends by the PWLT and EESC regressions for the 1984–1996 period, and significant positive EESC-based trends at 15–45 km and PWLTs at 34–45 km over the period 1997–2010. A clear structural similarity in the trends from both data sets (the OHP and GOZCARDS) is visible for both periods, although some differences in the PWLTs are found in the middle and lower stratosphere after 1997. This could be due to the differences in the two data sets as the GOZCARDS data are zonally and latitudinally (over 10°, as available) averaged as compared to the OHP data set (average ozone at the OHP latitude) or a result of unknown issues at this time, which are worthy of further investigation in the future. However, the structure of vertical distribution of ozone trends derived from both data sets and the trend values from EESC in the whole stratosphere and that of PWLT in the upper stratosphere corroborate that the ozone recovery signal in the northern mid-latitudes and the regression method are robust.

In order to test the sensitivity in selecting the vertical levels (pressure or geometric altitude), we have also done an analysis using ozone anomalies in percent (without converting ozone VMR to number density) based on the GOZCARDS pressure grid (with six levels per decade change in pressure) and the results are shown in Figure 8 (b). The PWLT (blue) and EESC-based (green) trends are very similar to the corresponding trends estimated, on a vertical grid in km, between 1984 and 1996 as well as 1997 and 2010. However, there are slight differences in the lowermost stratosphere and in the upper stratosphere, which could be due to the difference in the altitude–pressure conversion.

As found from the total column ozone, the ozone profile measurements also show similar trends for the PWLT and EESC-based analyses before 1997, showing the influence of ODSs in decreasing ozone during that period. For 1997–2010, the ozone trends derived from the EESC-based model are smaller than those from PWLT model below 30 km, suggesting the impact of other factors in addition to the decrease of ODSs for the increase in ozone. Above 40 km, the significant positive trends can be attributed to EESC only. It reflects the impact of ODSs on the evolution of ozone in the upper stratosphere, where the amount of ozone is mainly determined by the processes linked to homogeneous chemistry. Therefore, this study shows signals of ozone recovery in the lower, middle and upper stratosphere at northern mid-latitudes.

4 Conclusions

This study analyses the long-term evolution of monthly mean ozone at a northern mid-latitude station. The analysis uses total column ozone data from the Dobson and SAOZ spectrometers and stratospheric ozone profiles from lidar, ozonesondes, SAGE II, HALOE and Aura MLS. The variations in ozone are studied using a multiple linear regression model including QBO, solar flux, aerosol optical thickness, heat flux, NAO and PWLT or EESC terms. The regression model can explain about 65 % of the observed variance of the total column ozone and about 60–70 % of the ozone variability in the 20–40 km altitude range during winter/spring, and about 20–40 % below 20 and above 40 km.

The explanatory parameters exhibit clear seasonality and vertical differences in their contributions to the observed ozone variability. The QBO explains ozone variability in the whole stratosphere during winter/spring, while a significant response of ozone to solar flux is observed mostly in the middle stratosphere and a small part in the lower and upper stratosphere in summer. The heat flux and NAO contributions are maximum in the lower stratosphere during winter/spring and winter, respectively.

The PWLT and EESC fits yield similar and significant column ozone trends of about -1.47 ± 0.27 and $-1.40 \pm 0.25\,\mathrm{DU\,yr^{-1}}$ prior to 1997. The column ozone trends from both regressions show significant positive values for 1997–2010, but slightly higher ozone trends are derived from PWLT model. Stratospheric ozone profiles at OHP also yield similar and significant EESC-based and PWLT trends of about $-0.5\,\%\,\mathrm{yr^{-1}}$ at 34–37 km and about $-0.8\,\%\,\mathrm{yr^{-1}}$ at 38–45 km over the period 1984–1996. The ozone trends based on PWLT and EESC regressions are significant, and are of order 0.3 and $0.1\,\%\,\mathrm{yr^{-1}}$, respectively, at 18–28 km over the period 1997–2010. In the 40–45 km range, EESC provides significant ozone trends of about $0.25\,\%\,\mathrm{yr^{-1}}$, and these are larger than the insignificant PWLTs. Analyses with the GOZCARDS zonal mean ozone data averaged over the latitude bands of 40–50°N also provide matching vertical trend values (on either an altitude or pressure grid) by two regressions for the period 1984–1996, by EESC regression in the whole stratosphere and by PWLT regression above 33 km

over the period 1997–2010. Continued work on the ozone recovery signal from various methods and data sets is recommended, especially in the lower stratosphere.

This analysis indicates that the decline of total column and stratospheric ozone before 1997 is mainly attributed to the positive ODS trends, consistent with previous studies. However, the significant increase in ozone after the mid-1990s is partly caused by the decrease in ODSs below 30 km, and suggests the influence of other parameters than the reduced ODS level there. In contrast, the influence of ODS still dominates above 40 km, inducing a noteworthy increase in ozone. Therefore, this study suggests that stratospheric ozone is recovering not only in the upper stratosphere, as shown by Steinbrecht et al. (2006), but also in the whole stratosphere at northern mid-latitudes.

Acknowledgements. We would like to thank J. M. Russell III for the HALOE ozone data. We thank Cathy Boonne and the ETHER team for maintaining the ETHER data cluster, and the staff at OHP for operating the ozone monitoring instruments. Work at the Jet Propulsion Laboratory, California Institute of Technology, was done under contract with the National Aeronautics and Space Administration (NASA). We also thank the NASA Langley Research Center (NASA-LaRC) and the NASA Langley Radiation and Aerosols Branch for providing SAGE II data, and the collaborative institutes of the NASA Langley Research Center for maintaining HALOE data. The ground-based ozone measurements were obtained as part of the NDACC and are publicly available (see http://www.ndacc.org). Reanalysis of the OHP lidar data was performed under the EU NORS contract. The Aura MLS and GOZCARDS data used in this effort were acquired as part of the activities of NASA's Science Mission Directorate, and are archived and distributed by the GES DISC. GOZCARDS is part of NASA's MEaSUREs (Making Earth System data records for Use in Research Environments) programme. This work was partly supported by funding from the GEOMON (Global Earth Observation and Monitoring of the atmosphere) European project.

Edited by: M. Van Roozendael

The publication of this article is financed by CNRS-INSU.

References

Appenzeller, C., Weiss, A. K., and Staehelin, J.: North Atlantic oscillation modulates total ozone winter trends, Geophys. Res. Lett., 27, 1131–1134, doi:10.1029/1999GL010854, 2000.

Andrews, D. G., Holton, J. R., and Leovy, C. B. (Eds.): Middle atmosphere dynamics, Academic Press, International Geophysics Series, 40, Orlando, USA, 1987.

Basher, R. E.: Review of the Dobson Spectrophotometer and Its Accuracy, WMO Global Ozone Research and Monitoring Project, Report No. 13, WMO, Geneva, December 1982.

Bojkov, R., Bishop, L., Hill, W., Reinsel, G., and Tiao, G.: A statistical trend analysis of revised dobson total ozone data over the Northern Hemisphere, J. Geophys. Res., 95, 9785–9807, 1990.

Brühl, C., Roland Drayson, S., Russell III, J. M., Crutzen, P. J., McInerney, J. M., Purcell, P. N., Claude, H., Gernandt, H., McGee, T. J., McDermid, I. S., and Gunson, M. R.: Halogen Occultation Experiment ozone channel validation, J. Geophys. Res., 101, 10217–10240, 1996.

Brunner, D., Staehelin, J., Maeder, J. A., Wohltmann, I., and Bodeker, G. E.: Variability and trends in total and vertically resolved stratospheric ozone based on the CATO ozone data set, Atmos. Chem. Phys., 6, 4985–5008, doi:10.5194/acp-6-4985-2006, 2006.

Dhomse, S., Weber, M., Wohltmann, I., Rex, M., and Burrows, J. P.: On the possible causes of recent increases in northern hemispheric total ozone from a statistical analysis of satellite data from 1979 to 2003, Atmos. Chem. Phys., 6, 1165–1180, doi:10.5194/acp-6-1165-2006, 2006.

Dobson, G. M. B.: Observers' handbook for the ozone spectrophotometer, in: Annals of the International Geophysical Year, V, Part 1, Pergamon Press, 46–89, New York, 1957.

Dobson, G. M. B.: Forty years research on atmospheric ozone at Oxford: a History, Appl. Optics, 7, 387–405, 1968.

Froidevaux, L., Jiang, Y. B., Lambert, A., Livesey, N. J., Read, W. G., Waters, J. W., Browell, E. V., Hair, J. W., Avery, M. A., McGee, T. J., Twigg, L. W., Sumnicht, G. K., Jucks, K. W., Margitan, J. J., Sen, B., Stachnik, R. A., Toon, G. C., Bernath, P. F., Boone, C. D., Walker, K. A., Filipiak, M. J., Harwood, R. S., Fuller, R. A., Manney, G. L., Schwartz, M. J., Daffer, W. H., Drouin, B. J., Cofield, R. E., Cuddy, D. T., Jarnot, R. F., Knosp, B. W., Perun, V. S., Snyder, W. V., Stek, P. C., Thurstans, R. P., and Wagner, P. A.: Validation of Aura Microwave Limb Sounder stratospheric ozone measurements, J. Geophys. Res., 113, D15S20, doi:10.1029/2007JD008771, 2008.

Froidevaux, L., Fuller, R. A., Schwartz, M. J., Anderson, J., Wang, R.: README Document for the Global OZone Chemistry And Related trace gas Data records for the Stratosphere (GOZCARDS) project, Reviewed by J. E. Johnson, Goddard Earth Sciences Data and Information Services Center (GES DISC), http://disc.gsfc.nasa.gov NASA Goddard Space Flight Center, Code 610.2, Greenbelt, MD 20771 USA, 2013.

Godin, S., Marchand, M., Hauchecorne, A., and Lefèvre, F.: Influence of Arctic polar ozone depletion on lower stratospheric ozone amounts at Haute-Provence Observatory (43.92° N, 5.71° E), J. Geophys. Res., 107, 8272, doi:10.1029/2001JD000516, 2002.

Godin-Beekmann, S., Porteneuve, J., and Garnier, A.: Systematic DIAL lidar monitoring of the stratospheric ozone vertical distribution at Observatoire de Haute-Provence (43.92° N, 5.71° E), J. Environ. Monitor., 5, 57–67, 2003.

Heese, B., Godin, S., and Hauchecorne, A.: Forecast and simulation of stratospheric ozone filaments: a validation of a high-resolution potential vorticity advection model by airborne ozone lidar measurements in winter 1998/1999, J. Geophys. Res., 106, 20011–20024, doi:10.1029/2000JD900818, 2001.

Hendrick, F., Pommereau, J.-P., Goutail, F., Evans, R. D., Ionov, D., Pazmino, A., Kyrö, E., Held, G., Eriksen, P., Dorokhov, V., Gil, M., and Van Roozendael, M.: NDACC/SAOZ UV-visible total ozone measurements: improved retrieval and comparison with correlative ground-based and satellite observations, Atmos. Chem. Phys., 11, 5975–5995, doi:10.5194/acp-11-5975-2011, 2011.

Huang, J., Higuchi, K., and Shabbar, A.: The relationship between the North Atlantic Oscillation and El Nino-Southern Oscillation, Geophys. Res. Lett., 25, 14, 2707–2710, 1998.

Hurrell, J. W., Kushnir, Y., Ottersen, G., and Visbeck, M. (Eds.): The North Atlantic Oscillation: Climatic Significance and Environmental Impact, Geophysical Monograph, Vol. 134, American Geophysical Union, Washington, DC, 279 pp., 2003.

Jones, A., Urban, J., Murtagh, D. P., Eriksson, P., Brohede, S., Haley, C., Degenstein, D., Bourassa, A., von Savigny, C., Sonkaew, T., Rozanov, A., Bovensmann, H., and Burrows, J.: Evolution of stratospheric ozone and water vapour time series studied with satellite measurements, Atmos. Chem. Phys., 9, 6055–6075, doi:10.5194/acp-9-6055-2009, 2009.

Kiesewetter, G., Sinnhuber, B.-M., Weber, M., and Burrows, J. P.: Attribution of stratospheric ozone trends to chemistry and transport: a modelling study, Atmos. Chem. Phys., 10, 12073–12089, doi:10.5194/acp-10-12073-2010, 2010.

Komhyr, W. D.: Electrochemical concentration cells for gas analysis, Ann. Geophys., 25, 203–210, 1969, http://www.ann-geophys.net/25/203/1969/.

Kuttippurath, J. and Nikulin, G.: A comparative study of the major sudden stratospheric warmings in the Arctic winters 2003/2004–2009/2010, Atmos. Chem. Phys., 12, 8115–8129, doi:10.5194/acp-12-8115-2012, 2012.

Kuttippurath, J., Lefèvre, F., Pommereau, J.-P., Roscoe, H. K., Goutail, F., Pazmiño, A., and Shanklin, J. D.: Antarctic ozone loss in 1979–2010: first sign of ozone recovery, Atmos. Chem. Phys., 13, 1625–1635, doi:10.5194/acp-13-1625-2013, 2013.

Livesey, N. J., Read, W. G., Froidevaux, L., Lambert, A., Manney, G. L., Pumphrey, H. C., Santee, M. L., Schwartz, M. J., Wang, S., Cofeld, R. E., Cuddy, D. T., Fuller, R. A., Jarnot, R. F., Jiang, J. H., Knosp, B. W., Stek, P. C., Wagner, P. A., and Wu, D. L.: Earth Observing System (EOS) Aura Microwave Limb Sounder (MLS) Version 3.3 Level 2 data quality and description document, PL D-33509, Jet Propulsion Laboratory California Institute of Technology, Pasadena, California, 91109–8099, 2011.

Mäder, J. A., Staehelin, J., Brunner, D., Stahel, W. A., Wohltmann, I., and Peter, T.: Statistical modeling of total ozone: Selection of appropriate explanatory variables, J. Geophys. Res, 112, D11108, doi:10.1029/2006JD007694, 2007.

Nair, P. J., Godin-Beekmann, S., Pazmiño, A., Hauchecorne, A., Ancellet, G., Petropavlovskikh, I., Flynn, L. E., and Froidevaux, L.: Coherence of long-term stratospheric ozone vertical distribution time series used for the study of ozone recovery at a northern mid-latitude station, Atmos. Chem. Phys., 11, 4957–4975, doi:10.5194/acp-11-4957-2011, 2011.

Nair, P. J., Godin-Beekmann, S., Froidevaux, L., Flynn, L. E., Zawodny, J. M., Russell III, J. M., Pazmiño, A., Ancellet, G., Steinbrecht, W., Claude, H., Leblanc, T., McDermid, S., van Gijsel, J. A. E., Johnson, B., Thomas, A., Hubert, D., Lambert, J.-C., Nakane, H., and Swart, D. P. J.: Relative drifts and stability of satellite and ground-based stratospheric ozone profiles at NDACC lidar stations, Atmos. Meas. Tech., 5, 1301–1318, doi:10.5194/amt-5-1301-2012, 2012.

Newchurch, M. J., Yang, E.-S., Cunnold, D. M., Reinsel, G. C., and Zawodny, J. M.: Evidence for slowdown in stratospheric ozone loss: First stage of ozone recovery, J. Geophys. Res., 108, 4507, doi:10.1029/2003JD003471, 2003.

Pommereau, J. P. and Goutail, F.: Stratospheric O_3 and NO_2 observations at the southern polar circle in summer and fall 1988, Geophys. Res. Lett., 15, 895–897, doi:10.1029/GL015i008p00895, 1988.

Press, W. H., Flannery, B. P., Teukolsky, S. A., and Vetterling, W. T. (Eds.): Numerical Recipes, Cambridge University Press, Cambridge, UK, 504–508, 1989.

Rienecker, M. M., Suarez, M. J., Gelaro, R., Todling, R., Bacmeister, J., Liu, E., Bosilovich, M. G., Schubert, S. D., Takacs, L., Kim, G.-K., Bloom, S., Chen, J., Collins, D., Conaty, A.,da Silva, A., Gu, W., Joiner, J., Koster, R. D., Lucchesi, R., Molod, A., Owens, T., Pawson, S., Pegion, P., Redder, C. R., Reichle, R., Robertson, F. R., Ruddick, A. G., Sienkiewicz, M., and Woollen, J.: MERRA – NASA's modern-era retrospective analysis for research and applications, J. Climate, 24, 3624–3648, doi:10.1175/JCLI-D-11-00015.1, 2011.

Reinsel, G. C., Tiao, G. C., Wuebbles, D. J., Kerr, J. B., Miller, A. J., Nagatani, R. M., Bishop, L., and Ying, L. H.: Seasonal trend analysis of published ground-based and TOMS total ozone data through 1991, J. Geophys. Res., 99, 5449–5464, doi:10.1029/93JD03517, 1994.

Reinsel, G. C., Weatherhead, E. C., Tiao, G. C., Miller, A. J., Nagatani, R. M., Wuebbles, D. J., and Flynn, L. E.: On detection of turnaround and recovery in trend for ozone, J. Geophys. Res., 107, 4078, doi:10.1029/2001JD000500, 2002.

Reinsel, G. C., Miller, A. J., Weatherhead, E. C., Flynn, L. E., Nagatani, R. M., Tiao, G. C., and D. J. Wuebbles: Trend analysis of total ozone data for turnaround and dynamical contributions, J. Geophys. Res., 110, D16306, doi:10.1029/2004JD004662, 2005.

Russell, J. M., Gordley, L. L., Park, J. H., Drayson, S. R., Hesketh, W. D., Cicerone, R. J., Tuck, A. F., Frederick, J. E., Harries, J. E., and Crutzen, P. J.: The Halogen Occultation Experiment, J. Geophys. Res., 98, 10777–10797, 1993.

Salby, M., Titova, E., and Deschamps, L.: Rebound of Antarctic ozone, Geophys. Res. Lett., 38, L09702, doi:10.1029/2011GL047266, 2011.

Sato, M., Hansen, J., McCormick, M., and Pollack, J.: Stratospheric Aerosol Optical Depths, 1850–1990, J. Geophys. Res., 98, 22987–22994, 1993.

Staehelin, J., Kegel, R., and Harris, N. R. P.: Trend analysis of the homogenized total ozone series of Arosa (Switzerland), 1926–1996, J. Geophys. Res., 103, 8389–8399, doi:10.1029/97JD03650, 1998.

Smit, H. G. J., Straeter, W., Johnson, B. J., Oltmans, S. J., Davies, J., Tarasick, D. W., Hoegger, B., Stübi, R., Schmidlin, F. J., Northam, T., Thompson, A. M., Witte, J. C., Boyd, I., and Posny, F.: Assessment of the performance of ECC ozonesondes under quasi flight conditions in the environmental simulation chamber: insights from the Juelich Ozone Sonde Intercomparison Experiment (JOSIE), J. Geophys. Res., 112, D19306, doi:10.1029/2006JD007308, 2007.

Steinbrecht, W., Hassler, B., Claude, H., Winkler, P., and Stolarski, R. S.: Global distribution of total ozone and lower stratospheric temperature variations, Atmos. Chem. Phys., 3, 1421–1438, doi:10.5194/acp-3-1421-2003, 2003.

Steinbrecht, W., Claude, H., Schönenborn, F., McDermid, I. S., Godin, S., Song, T., Swart, D. P. J., Meijer, Y. J., Bodeker, G. E., Connor, B. J., Kämpfer, N., Hocke, K., Calisesi, Y., Schneider, N., de la Noë, J., Parrish, A. D., Boyd, I. S., Brühl, C., Steil, B., Giorgetta, M. A., Manzini, E., Thomason, L. W., Zawodny, J. M., McCormick, M. P., Russell III, J. M., Bhartia, P. K., Stolarski, R. S., and Hollandsworth-Frith, S. M.: Long-term evolution of upper stratospheric ozone at selected stations of the Network for the Detection of Stratospheric Change (NDSC), J. Geophys. Res., 111, D10308, doi:10.1029/2005JD006454, 2006.

Steinbrecht, W., Claude, H., Schönenborn, F., McDermid, I. S., Leblanc, T., Godin-Beekmann, S., Keckhut, P., Hauchecorne, A., Van Gijsel, J. A. E., Swart, D. P. J., Bodeker, G. E., Parrish, A., Boyd, I. S., Kämpfer, N., Hocke, K., Stolarski, R. S., Frith, S. M., Thomason, L. W., Remsberg, E. E., Von Savigny, C., Rozanov, A., and Burrows, J. P.: Ozone and temperature trends in the upper stratosphere at five stations of the Network for the detection of atmospheric composition change, Int. J. Remote Sens., 30, 3875–3886, doi:10.1080/01431160902821841, 2009.

Steinbrecht, W., Köhler, U., Claude, H., Weber, M., Burrows, J. P., and van der A, R. J.: Very high ozone columns at northern mid latitudes in 2010, Geophys. Res. Lett., 38, L06803, doi:10.1029/2010GL046634, 2011.

Storch, H. V. and Zwiers, F. W.: Statistical Analysis in Climate Research: Fitting Statistical Models, Cambridge University Press, Cambridge, UK, 1999.

Vigouroux, C., De Mazière, M., Demoulin, P., Servais, C., Hase, F., Blumenstock, T., Kramer, I., Schneider, M., Mellqvist, J., Strandberg, A., Velazco, V., Notholt, J., Sussmann, R., Stremme, W., Rockmann, A., Gardiner, T., Coleman, M., and Woods, P.: Evaluation of tropospheric and stratospheric ozone trends over Western Europe from ground-based FTIR network observations, Atmos. Chem. Phys., 8, 6865–6886, doi:10.5194/acp-8-6865-2008, 2008.

Vyushin, D. I., Fioletov, V. E., and Shepherd, T. G.: Impact of long-range correlations on trend detection in total ozone, J. Geophys. Res., 112, D14307, doi:10.1029/2006JD008168, 2007.

Vyushin, D. I., Shepherd, T. G., and Fioletov, V. E.: On the statistical modeling of persistence in total ozone anomalies, J. Geophys. Res., 115, D16306, doi:10.1029/2009JD013105, 2010.

Wang, P. H., Cunnold, D. M., Trepte, C. R., Wang, H. J., Jing, P., Fishman, J., Brackett, V. G., Zawodney, J. M., and Bodeker, G. E.: Ozone variability in the midlatitude upper troposphere and lower stratosphere diagnosed from a monthly SAGE II climatology relative to the tropopause, J. Geophys. Res., 111, D21304, doi:10.1029/2005JD006108, 2006.

Wang, R., Froidevaux, L., Anderson, J., Fuller, R. A., Bernath, P. F., McCormick, M. P., Livesey, N. J., Russell III, J. M., Walker, K. A., and Zawodny, J. M.: GOZCARDS Merged Data for Ozone Monthly Zonal Means on a Geodetic Latitude and Pressure Grid,version 1.01, Greenbelt, MD, USA:NASA Goddard Earth Science Data and Information Services Center, Accessed 02 May, 2013 at doi:10.5067/MEASURES/GOZCARDS/DATA3006, 2013.

Weber, M., Dikty, S., Burrows, J. P., Garny, H., Dameris, M., Kubin, A., Abalichin, J., and Langematz, U.: The Brewer–Dobson circulation and total ozone from seasonal to decadal time scales, Atmos. Chem. Phys., 11, 11221–11235, doi:10.5194/acp-11-11221-2011, 2011.

Weiss, A. K., Staehelin, J., Appenzeller, C., and Harris, N. R. P.: Chemical and dynamical contributions to ozone profile trends of the Payerne (Switzerland) balloon soundings, J. Geophys. Res., 106, 22685–22694, doi:10.1029/2000JD000106, 2001.

WMO (World Meteorological Organization): Scientific assessment of ozone depletion: 2006, Global Ozone Research and Monitoring Project, Rep. 50, Geneva, Switzerland, 572 pp., 2007.

WMO: Scientific assessment of ozone depletion: 2010, Global Ozone Research and Monitoring Project, Rep. 52, Geneva, Switzerland, 516 pp., 2011.

Wohltmann, I., Lehmann, R., Rex, M., Brunner, D., and Mäder, J. A.: A process-oriented regression model for column ozone, J. Geophys. Res., 112, D12304, doi:10.1029/2006JD007573, 2007.

Yang, E.-S., Cunnold, D. M., Salawitch, R. J., McCormick, M. P., Russell III, J., Zawodny, J. M., Oltmans, S., and Newchurch, M. J.: Attribution of recovery in lower-stratospheric ozone, J. Geophys. Res., 111, D17309, doi:10.1029/2005JD006371, 2006.

Zanis, P., Maillard, E., Staehelin, J., Zerefos, C., Kosmidis, E., Tourpali, K., and Wohltmann, I.: On the turnaround of stratospheric ozone trends deduced from the reevaluated Umkehr record of Arosa, Switzerland, J. Geophys. Res., 111, D22307, doi:10.1029/2005JD006886, 2006.